International Journal of Nanomedicine

Dovepress
open access to scientific and medical research

Open Access Full Text Article

ORIGINAL RESEARCH

B16 Membrane-Coated Vesicles for Combined Photodynamic Therapy and Immunotherapy Shift Immune Microenvironment of Melanoma

Yuqian Wang[1]*, Zhilong Zhao[2]*, Chenlu Liu[3], Miao Hao[1], Chenfei Kong[1], Xiaoming Zhao[1], Yiyao Gao[1], Yucheng Zhang[1], Wanxing Cui[4], Congxiao Zhang[2], Jinlan Jiang[1]

[1]Scientific Research Center, China-Japan Union Hospital, Jilin University, Changchun, 130031, People's Republic of China; [2]Department of Stomatology, The First Hospital of Jilin University, Changchun, 130031, People's Republic of China; [3]Biobank, China-Japan Union Hospital, Jilin University, Changchun, 130031, People's Republic of China; [4]Medstar Georgetown Transplant Institute, Georgetown University Hospital, Washington, DC, 20007, USA

*These authors contributed equally to this work

Correspondence: Congxiao Zhang; Jinlan Jiang, Email zhangcongxiao@jlu.edu.cn; jiangjinlan@jlu.edu.cn

Introduction: Coating of nanomedicine with cell membranes has attracted increasing attention as it can boost biocompatibility and improve the efficiency of treatment. Herein, we prepared innovative tumor cell-membrane-coated vesicles based on photodynamic therapy (PDT) drug indocyanine green (ICG) and explore the effect on melanoma in vitro and in vivo.

Methods: ICG was coated with B16 cell membranes (I@BM NVs) by sonication and extrusion, and the morphological characteristics of I@BM NVs were evaluated by transmission electron microscopy (TEM) and NP-tracking analysis. Homologous cellular uptake was evaluated by flow cytometry (FCM) after staining by DiD dye. Cellular cytotoxicity was evaluated by cell counting kit-8 assay and the anti-tumor effect in vitro was assessed by FCM and western blotting. The anti-tumor effect in vivo was evaluated in a B16 xenograft model in mice. The tumor micro-environment was investigated by FCM and real-time PCR.

Results: The vesicles are stable and uniform in nature, and show strong homologous targeting in vivo and in vitro. The vesicles can generate reactive oxygen species to induce apoptosis of B16 cells under near-infrared irradiation. Furthermore, the I@BM NVs induce a significant anti-tumor response in vivo, and perform better with respect to both tumor growth inhibition and lifespan extension. Analysis of immunocytes in the tumor microenvironment showed significant reductions in numbers of myeloid-derived suppressor cells and tumor-associated M2 macrophages in mice in the I@BM NVs group. This was accompanied by significant increases in numbers of M1 macrophages and proliferative $CD4^+/CD8^+$ T cells. Expression levels of IFN-γ and IL-2 increased in the I@BM NVs group, while expression of TGF-β and IL-10 decreased.

Conclusion: The results show that the I@BM NVs are feasible drugs for the treatment of melanoma by inducing cell apoptosis under NIR and shifting the immunosuppressive tumor microenvironment in vivo.

Keywords: melanoma, vesicles, tumor microenvironment, photodynamic therapy, immunotherapy

Introduction

Cancer has long threatened human life and is the second leading cause of death worldwide. Malignant melanoma is a tumor type with a poor prognosis, often occurring on the skin or in the oral cavity. Although malignant melanoma accounts for a small proportion of all skin cancers, it has a high mortality rate.[1,2] Moreover, owing to the aggressiveness of malignant melanoma, patients have poor prognosis after surgery in the advanced stage. Photodynamic therapy (PDT) has been shown by some research to inhibit tumor growth efficiently.[3] Approved by the Food and Drug Administration for clinical applications, ICG has superior PDT effects and is a safe and commonly used NIR fluorescent drug.[4] However, its rapid in vivo clearance and photo-degradation have limited its application.[5]

Received: 13 September 2021
Accepted: 1 February 2022
Published: 22 February 2022

Graphical Abstract

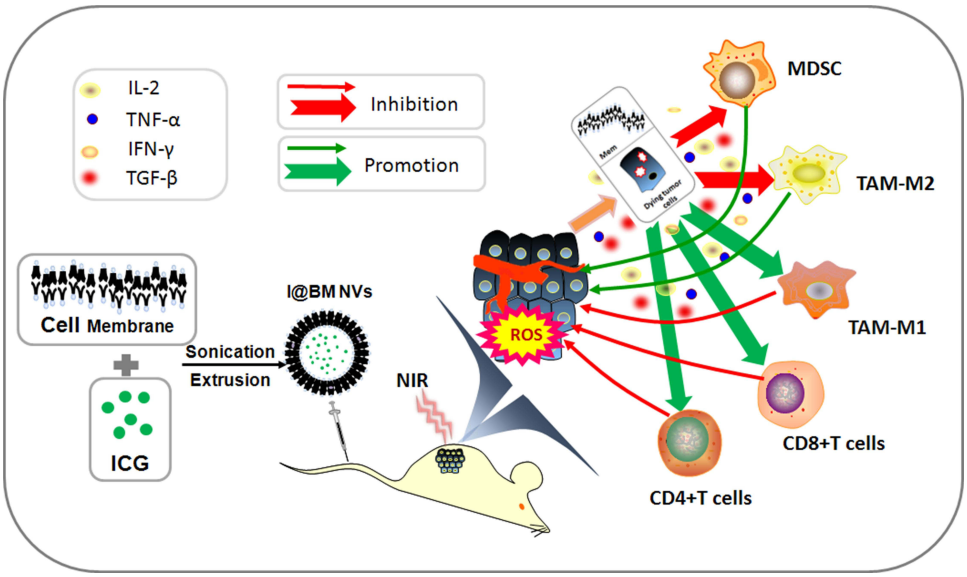

In order to improve clinical effectiveness and stability, more and more scholars have loaded ICG into different nanomaterials to overcome these shortcomings. Zhang et al demonstrated that composite mesoporous silica nanoparticles (MSN(Mn))-ICG/ dacarbazine (DTIC) could act as a multifunctional nanoplatform to accomplish a supernal efficient chemo-photothermal combined therapy for malignant melanoma treatment.[6] The efficiency of combined photothermal therapy–PDT using ICG-loaded gold nano-bipyramids was also validated against B16-F10 melanoma.[7] What's more, endogenous human serum albumin (HSA) and poly (lactic-glycolic acid copolymer) with biodegradable properties are also used as delivery systems for ICG.[8,9] However, due to non-natural surface characteristics, these artificial carriers are generally identified by the body's immune system, leading to toxic immune response and rapid clearance.

Recently, more and more researchers have used cell membranes as carriers for drug delivery systems. Cell membrane-derived vesicles have special components such as proteins and lipids, which distinguish them from other nanoplatforms.[10,11] The application of membrane-labeled vesicles can effectively protect the biological activity of tumor surface-adhesion molecules, enabling membrane-labeled NVs to specifically target tumors and maintain long-term blood circulation.[12,13]

Cancer cell membranes with specific proteins on the surface have attracted much attention because of their homologous targeting functions. In addition, due to the presence of tumor-associated antigens on the surface of the cancer cell membrane, it can activate T cells to trigger cellular immunity after being recognized by the immune system, so that the cancer cell membrane-coated nanoparticles can be used for immunotherapy. Recently, Jin et al[14] prepared biomimetic poly (lactic-co-glycolic acid)(PLGA) NPs coated with human cancer cell membrane fractions (CCMF) to form CCMF coated PLGA (CCMF-PLGA) NPs, which significantly reduced experimental metastasis in vivo. These effects were primarily due to the triggering of a higher percentage of CD8+ and CD4+ cytotoxic T-lymphocyte populations.

It has been shown that cell membrane-derived vesicles usually have been used to coat a hollow core structure composed of different material types and with different shapes, besides encapsulating small molecules within their interior.[11,15] However, hollow core materials' strong immunogenicity and difficulty in metabolism have always been the shortcomings of hollow core materials. Hollow core materials are accidentally cleared in the body after repeated administration, making hollow core materials a long way to go in clinical work.

Our group loaded free ICG into B16 cell vesicles to control the permeability of polyelectrolyte microcapsules, so that hydrophilic ICG can be loaded into membrane vesicles in a slow-release manner, thereby reducing the side effects of poor ICG water stability. Moreover, ICG could be released because of its potential to penetrate cell membranes and amphiphilicity. At the same time, the homologous targeting and immunotherapy of tumor cell membrane can enhance the PDT effect of ICG drugs. In this study, a simple and easy method was used to prepare nano-vesicles that could deliver a combination of immunotherapy and PDT to treat melanoma. Dynamic light scattering (DLS) showed that the prepared nano-vesicles had small particle size (~160nm). The nano-vesicles also showed high targeting efficacy through homologous targeting effects as indicated by the cellular uptake and animal studies. After 808-nm NIR laser treatment, the tumor cell-membrane-coated NVs based on ICG (I@BM NVs) generated plentiful ROS to induce cell apoptosis. Finally, efficient tumor growth suppression and a positive tumor microenvironment were achieved in a mouse melanoma model. Our results provide a direct theoretical basis for the application of membrane-coated NVs in the clinical treatment of melanoma and other malignant tumors.

Materials and Methods

Materials and Cell Lines

ICG, Cell Counting Kit-8 (CCK8), 1,1′-dioctadecyl-3,3,3′,3′-tetramethylindodicarbocyanine perchlorate (DiD), calcein-AM/propidium iodide (PI)/fluorescein isothiocyanate (FITC), phosphate-buffered saline (PBS), and BCA protein assay kit were obtained from Beyotime (China). Penicillin–streptomycin, fetal bovine serum (FBS), and high-glucose Dulbecco's modified Eagle medium (DMEM) were acquired from ThermoFisher (Waltham, MA, USA). RIPA lysis buffer was obtained from Beyotime Biotechnology (China). Antibody against gp100 was provided by BD Biosciences (USA). Antibody against Na^+/K^+-ATPase was purchased from GenScript (USA). Histone H3(H3) antibody, cytochrome c oxidase subunit IV(COXIV) antibody and glyceraldehyde-3-phosphate dehydrogenase (GAPDH) antibody were purchased from Proteintech Company (China). β-actin antibody was obtained from Santa Cruz Biotechnology (USA). Antibodies against caspase-9/cleaved caspase-9 were purchased from Thermo Fisher Scientific (USA). BAX antibody was obtained from Santa Cruz Biotechnology (USA). The 220-nm polycarbonate membranes were provided by Merck Millipore (Germany). B16, L929, and 4T1 cell lines were generous gifts from the National Engineering Laboratory of AIDS Vaccines of Jilin University,[16] and the use of the cell lines was approved by the institutional research ethics committee of China-Japan Union Hospital of Jilin University.

Cancer Cell Membrane Extraction

B16 cell membrane was prepared according to the previously published protocol with a few modifications.[19,20] Briefly, B16 cells were cultured in a 10-cm-diameter cell culture dish for 48 h. After being digested with trypsin, the cells were collected by centrifugation at 800 g for 5 min. Cells were counted and then washed with PBS (10 mM, pH = 7.4) at 4 °C and then stored at −40 °C. The B16 cells were then lysed using ultrasound and centrifuged at 3200 g for 10 min, and the supernatant was collected. The supernatant was then centrifuged at 15,000 g for 25 min to obtain the cell membranes.[17,18] These cell membranes were measured and then stored at −80 °C for further use.

Preparation and Characterization of B16 Membrane-Coated ICG NVs

ICG (25 μg) was dissolved in 1 mL of deionized water. B16 cell membranes extracted from 4×10^6 cells were added to 1 mL ICG aqueous solution (25 μg/mL) under sonication at a power of 39 W and frequency of 20 kHz for 10 min to form B16 membrane-coated ICG NVs (I@BM NVs). After the solution had been sonicated, the sediment was collected by centrifugation at 15,000 g for 30 min at 4 °C. The sediment was washed thoroughly with PBS and then centrifuged again to collect the precipitate. After being dissolved in a 200μL of PBS, the particles were filtered through a 220-nm membrane for 20 times. The medium diameter, size distribution of the obtained NVs were detected by a Nanosight (NS300, Malvern Panalytical, Malvern, UK). The encapsulation efficiencies (EE) of ICG of I@BM NVs were determined. The NVs after precipitation were isolated from the aqueous medium by ultracentrifugation (15,000 r/min, 30 min). A UV/vis spectrometer (F-4600; Shimadzu, Tokyo, Japan) was used to measure the free ICG of the supernatant at an λmax of 784 nm. The EE of ICG-loaded NVs were calculated using the formula $EE\ (\%) = (ICG_{Total} - ICG_{Free})/ICG_{Total} \times 100\%$.

I@BM NVs were observed by transmission electron microscopy (TEM; JEM-1400, JEOL, Japan) by first glow-discharging carbon-coated 400 square mesh copper grids (Beijing Zhongjingkeyi Technology). Vesicles at 1 mg/mL were left on the grid for 1 min before being washed off with 10 drops of water. Grids were then negatively stained with three drops of 2% uranyl acetate (Sigma Aldrich). Excess solution was wicked away with absorbent paper, and the samples were imaged using a Tecnai G2 Sphera (FEI) microscope at 200 kV. Moreover, the zeta potentials and DLS of I@BM NVs were evaluated every day using a Mastersizer 3000 analyzer (Malvern, UK) for up to 7 days.

In vitro Release Profile Study

To investigate the ICG drug release of I@BM NVs in vitro, 2 mL I@BM NVs aqueous solution (containing 25 ug ICG per mL) was injected into a dialysis bag (M.W. 3500 Da) and dialyzed against phosphate-buffered saline (PBS, pH = 7.4) at room temperature under persistent shaking without the light. At each scheduled time point of 6 days, drug concentration in dialysate was surveyed by UV spectrophotometer (F-4600; Shimadzu, Tokyo, Japan). During the experiment, the total volume of dialysate was maintained at 50 mL.

Photostability of I@BM NVs

The degradation of I@BM NVs and free ICG was illuminated at room temperature to evaluate the photostability under visible light. The I@BM NVs and free ICG were diluted with PBS solution to a concentration of 25 μg/mL and were injected into a 6-well plate for experiment. The photostability test was conducted for 6 days. At each scheduled time point of 6 days, the fluorescence intensity of each sample was measured using a UV spectrophotometer with excitation and emission wavelengths of 714 nm and 780 nm, respectively. The fluorescence signal intensity was normalized for the quantitative analysis.

Cancer Cell Membrane Protein Characterization

The membrane proteins of I@BM NVs were characterized by sodium dodecyl sulfate polyacrylamide gel electrophoresis (SDS-PAGE). RIPA lysis buffer was added to the B16 cells, B16 cell membranes, ICG, and I@BM NVs. The samples were lysed for 15 min and subjected to ultrasonication for 1 min. Supernatants were collected after centrifugation at 13,500 g for 20 min at 4 °C and analyzed using a BCA assay kit (Beyotime, China). Following the addition of 5× loading buffer, samples were heated to 100 °C for 5 min. A marker, B16 membrane, and I@BM NVs were added to the wells of a 10% SDS-PAGE gel. After electrophoresis, the SDS-PAGE gel was stained with Coomassie Blue for 2 h, then placed in water and heated for 1 h for decoloration. Western blotting was used to evaluate expression of Na^+/K^+-ATPase and gp100. After 1 h of blocking, polyvinylidene fluoride membranes were treated with anti-Na^+/K^+-ATPase, anti-gp100, anti-H3, anti-GAPDH and anti-COXIV, followed by IRDye® 800CW-conjugated secondary IgG. The protein signals were visualized and analyzed using an Odyssey Infrared Imaging System.

Verification of I@BM NVs Homologous Targeting

B16 cells, HeLa cells, 4T1 cells, and L929 cells were incubated in Petri dishes. After 12 h, the cells were digested and centrifuged. DiD (10μM) and I@BM NVs (0.2mg mem vesicles containing 50 μg ICG in 200 μL saline) were co-incubated in the dark for 10 min, washed with PBS, and centrifuged at 15,000 g for 10 min to obtain DiD-stained I@BM NVs (DiD-I@BM NVs). DiD-I@BM NVs and PBS were separately added to the four cell types (each 2×10^6 cells). After shaking for 3 h in a 37 °C constant-temperature shaker, the cells were washed and harvested in centrifuge tubes, and a flow cytometer (BD FACS Calibur) was used to measure the fluorescence intensity of DiD. Data were analyzed using FlowJo software.

In vitro Cytotoxicity Assay of I@BM NVs

The cytotoxicity of I@BM NVs was measured by CCK-8 (Dojindo, Japan) assay. After seeding of B16 cells in a 96-well plate (2×10^4 cells/well) and culturing for 24 h, ICG and I@BM NVs solutions were diluted to the required concentration and added to the 96-well plate for a further 24 h. After irradiation of the ICG and I@BM NV solutions with 808-nm NIR at a power of 2 w/cm^2 for 5 min, the 96-well plate was placed in a cell incubator for 3 h. Then, CCK-8 (10 μL) reagent was added to each well. After incubation for 2 h, the absorbances of samples at 450 nm were measured using a microplate reader (ELx-800, BioTek Instruments, USA).

In vitro Apoptosis Assay of I@BM NVs

B16 cells were seeded in a six-well plate at a density of 8×10^5 cells/well and incubated overnight in DMEM containing 10% FBS. PBS, membrane vesicles (0.1mg), ICG (25μg), and I@BM NVs (0.1mg mem vesicles containing 25 μg ICG) were added to respective wells. After 3 h incubation, the cells were irradiated for 4 min by NIR. After another 3 h, trypsin-free EDTA centrifugation was performed, and the cells were harvested. Cells were stained with an annexin V-FITC/PI apoptosis detection kit and incubated in the dark, and then apoptotic cells were detected with a flow cytometer. Moreover, western blot analysis was used to evaluate the protein expression of caspase-9/cleaved caspase-9 and BAX.

Therapeutic Experiments in Tumor-Bearing Mice

Female BALB/c nude mice and C57/BL/6 mice, 6–8 weeks old (Beijing Huafukang Biology Technology Co., Ltd., China), were used in this study. All animal procedures were conducted in strict accordance with the National Institutes of Health Guide for the Care and Use of Laboratory Animals and were approved by the University Committee on the Use and Care of Animals of Jilin University of China.

B16 melanoma cancer cells (1×10^6) were implanted subcutaneously into the right back flanks of mice at day 0. Tumor size was measured every 2 days, and the tumor volume was calculated as (length×width^2)/2. For the tumor retention study, the average tumor size was allowed to reach 100 mm^3, after which saline as the negative control (n = 3), ICG (50 μg in 50 μL saline, n = 3), and DiD-labeled NVs (0.2mg mem vesicles containing 50 μg ICG in 50 μL saline, n = 3) were administered to mice. Each animal received one tail vein injection and was imaged using a Xenogen IVIS 200 system at various time points, including 0 min, 1 h, 3 h, 6 h, and 24 h, with the same acquisition time and filter settings. Acquired images were analyzed using Xenogen Living Image 3.0 to quantify the fluorescence intensity of the tumors and to determine tumor retention percentages.

To assess the therapeutic effect of the NVs, saline (50μL), ICG (50 μg in 50 μL saline), Mem vesicles (0.2 mg in 50 μL saline), and I@BM NVs (0.2mg mem vesicles containing 50 μg ICG in 50 μL saline) were administered to mice bearing tumors with an average volume of 100 mm^3 by the tail vein three times at 1-week intervals. The tumor inhibition rate (%) was calculated as follows: (average tumor volume of PBS group – average tumor volume of experimental group)/average tumor volume of PBS group × 100%. Mice were sacrificed at week 4 after inoculation with B16 cells. Survival of mice was monitored for ~50 days. The liver and kidney were collected and subjected to hematoxylin and eosin (H&E) staining to evaluate the biotoxicity of the nanoformulations in vivo.

Analysis of Immune Cells in Tumors

Mice were euthanized, and their tumor tissues and main organs were removed. One gram of tissue was taken from each group of tumors and placed in serum-free 1640 medium for extraction of cells from tumor tissues. First, the tumor tissue was cut into small pieces, Liberase (Roche) was added to a final concentration of 0.04 mg/mL, and the tissue was digested in an incubator at 37 °C, 5% carbon dioxide, for 2 h. After the tissue had been fully ground, the cells were washed and counted to 1×10^7 cells/mL. Then, 100 μL (1×10^6) cells were added to solution diluted antibody for staining, such as PE anti-mouse CD11b (Biolegend), APC anti-mouse CD206 (Biolegend), FITC anti-mouse F4/80 (Biolegend), and APC anti-mouse Gr-1 (Biolegend), to analyze myeloid-derived suppressor cells (MDSCs) and tumor-associated macrophages (TAMs) in tumors. APC anti-mouse CD8a (Biolegend), PE-Cy7 anti-mouse CD4 (Biolegend), and PE anti-mouse Ki67 were also used to stain the cells, in order to analyze proliferative T cells in the tumor microenvironment. Flow cytometry was used to wash and analyze the cells, and a Mouse Regulatory T Cell Staining Kit #1 (eBioscience) was used to detect regulatory T cells (Tregs) according to the manufacturer's instructions.

Quantification of Intra-Tumoral Cytokine Expression by Quantitative Real-Time PCR (qRT-PCR)

According to the manufacturer's protocol, a RNeasy mini kit (Qiagen, CA) was used to extract total RNA from tumor tissues. An ABI StepOne Plus system (Applied Biosystems, USA) and SYBR Green Master Mix kit (Thermo Fisher, USA) were used to detect IFN-γ, IL-2, TGF-β, and IL-10 mRNA levels by qRT-PCR. β-actin was used as an internal control.

Statistical Analyses

All experimental data are expressed as mean ± standard deviation. One-way analysis of variance was used to analyze the data. Unpaired *t*-test was used to assess the statistical significance of the differences between groups. $P < 0.05$ was considered significant. All statistical analyses were performed using GraphPad Prism software.

Results and Discussion

Preparation and Characterization of I@BM NVs

The encapsulation efficiency of ICG in the I@BM NVs was about 40%-45%, which means that 0.1mg mem vesicles can encapsulate at most 25μg ICG. TEM observations of the I@BM NVs showed obvious membrane-structured NVs with rounded morphology (Figure 1A). According to the DLS results, the mean diameter of the I@BM NVs was 163 nm ± 28.5 nm and I@BM NVs had a relatively narrow particle size distribution (80% of NPs had a diameter < 230 nm) (Figure 1B), consistent with the TEM results. The ultraviolet–visible light absorption spectrum of I@BM NVs showed a unique absorption peak similar to that of ICG (Figure 1C). The slight UV absorption shift at λmax of 780 nm was

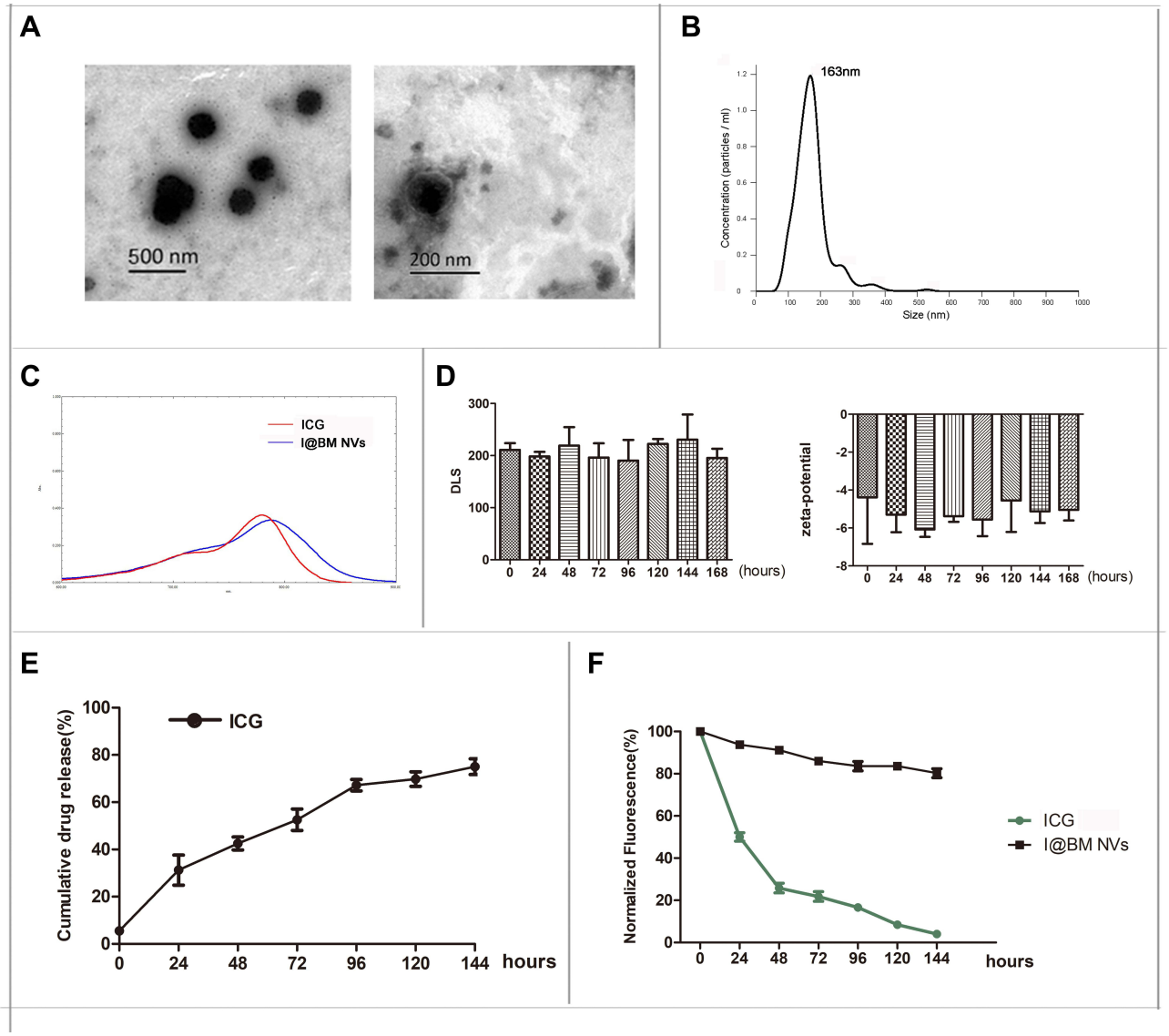

Figure 1 Synthesis and characterization of I@BM NVs. (**A**) TEM image of I@BM NVs. (**B**) PDI of I@BM NVs. (**C**) UV/Vis spectra of free ICG, and I@BM NPs in PBS. (**D**) Zeta potentials and DLS of I@BM NVs at different time point. (**E**) The release profile of ICG from I@BM NVs. (**F**) The photostability of free ICG and I@BM NVs. Data are expressed as mean ± SD.

observed which showed that ICG had been successfully loaded in the B16 membrane vesicles.[19,20] We placed the NVs in PBS at 4 °C for 168 h to observe their stability. The DLS results showed that the size of the NVs did not change significantly (Figure 1D). In addition, the electrical potential of the NVs remained stable These results indicate that the synthesized NVs had excellent stability (Figure 1D).

The in vitro release characteristics of ICG from I@BM NVs were shown in Figure 1E. During the first 24 h, a rapid release occurred with a cumulative release of 30%, which was mainly attributed to the initial burst of free ICG in vesicles. Subsequently, from 24 to 144 h, a relatively slow release occurred with a cumulative release up to 80%. The results indicated that I@BM NVs achieved sustained release of ICG, which was a critical factor for its PDT application.

To examine whether the encapsulation of the ICG within the membrane vesicles could enhance the photostability of the ICG fluorescence against external light, free ICG and I@BM NVs were exposed to visible light for 6 days, and the fluorescence intensity was analyzed. The I@BM NVs exposed to the visible light maintained their fluorescence intensity over the 6-day period. However, after 1 day of exposure to visible light, the fluorescence intensity of the free ICG solution was reduced to less than 50% of its initial value and was less than 1/2 of I@BM NVs (Figure 1F).

Validation of B16 Cell Membrane Proteins and Homologous Targeting of I@BM NVs

The protein profiles of the I@BM NVs were verified to confirm the successful functionalization of NVs with B16 cell membrane proteins. The NVs showed similar protein profiles to those of the B16 cell membranes, according to protein gel electrophoresis (Figure 2A). Western blotting analysis was proceeded with a battery of intracellular and membrane protein so as to verify the presence of membrane specific antigens on the I@BM NVs (Figure 2B). Na+/K+-ATPase, as cell membrane-specific proteins markers, is abundantly present in the I@BM NVs. Glycoprotein 100 (gp100) is a widely reported melanoma-associated antigen with a significant role in cell homologous targeting.[21] Gp100 has similar expression level on the I@BM NVs as B16 cell extraction. However, other protein markers for the cytoplasm (GAPDH), mitochondria (COXIV), and nucleus (H3) were lowly expressive on the I@BM NVs, demonstrating extracted membrane with more membrane proteins and less intracellular proteins. These results indicated that most of the membrane proteins were retained during preparation and that the I@BM NVs were successfully prepared.[22,23]

To quantify the difference in absorption, flow cytometry was performed to evaluate I@BM NVs targeting B16 cells, mouse diploid cells (L929 mouse fibroblasts), and other cancer cells (4T1 mouse breast cancer cells and HeLa human cervical cancer cells) (Figure 2C). The results showed that compared with mouse diploid cells and other cancer cells, the average signal intensity of B16 cells increased approximate about 10-fold, demonstrating that I@BM NVs prepared with B16 cell membrane showed increased targeting of source cells.

ROS Generation

The generation of ROS can be detected using a ROS probe kit (Figure 3A). As the combination of ROS and ROS probes produces specific-wavelength fluorescence, we used flow cytometry to detect the ROS content of cells after light treatment. As shown in Figure 3A, the fluorescence intensity of B16 cells incubated with NVs was 2.3 times that of cells treated with free ICG. This may have been due to the homologous targeting ability of B16 cell membrane, which made more NVs entering B16 cells.[24,25] The results further illustrated that the NVs exhibit stronger homology targeting than free ICG.

Photocytotoxicity of I@BM NVs

Cells were treated with different concentrations of NVs for 24 h and irradiated with an 808-nm laser with a power of 2 W/cm^2 for 4 min; then, the lethality of the I@BM NVs to the cells was evaluated. Theoretically, the presence of B16 cell membrane should have increased the rate of uptake of NVs by B16 cells. The cell viability measurements after irradiation are shown in Figure 3B. After 4 min of light excitation, B16 cell viability decreased in a concentration-dependent manner. The viability of cells treated with free ICG+laser (containing 35 μg/mL ICG) was about 20%, and cells treated with I@BM NVs+laser (containing ~35 μg/mL ICG) resulted in about 95% cell death. These results can be attributed to the high cellular uptake rate of I@BM NVs, the increase in ICG photostability, and the mount of ROS produced when cells are damaged.

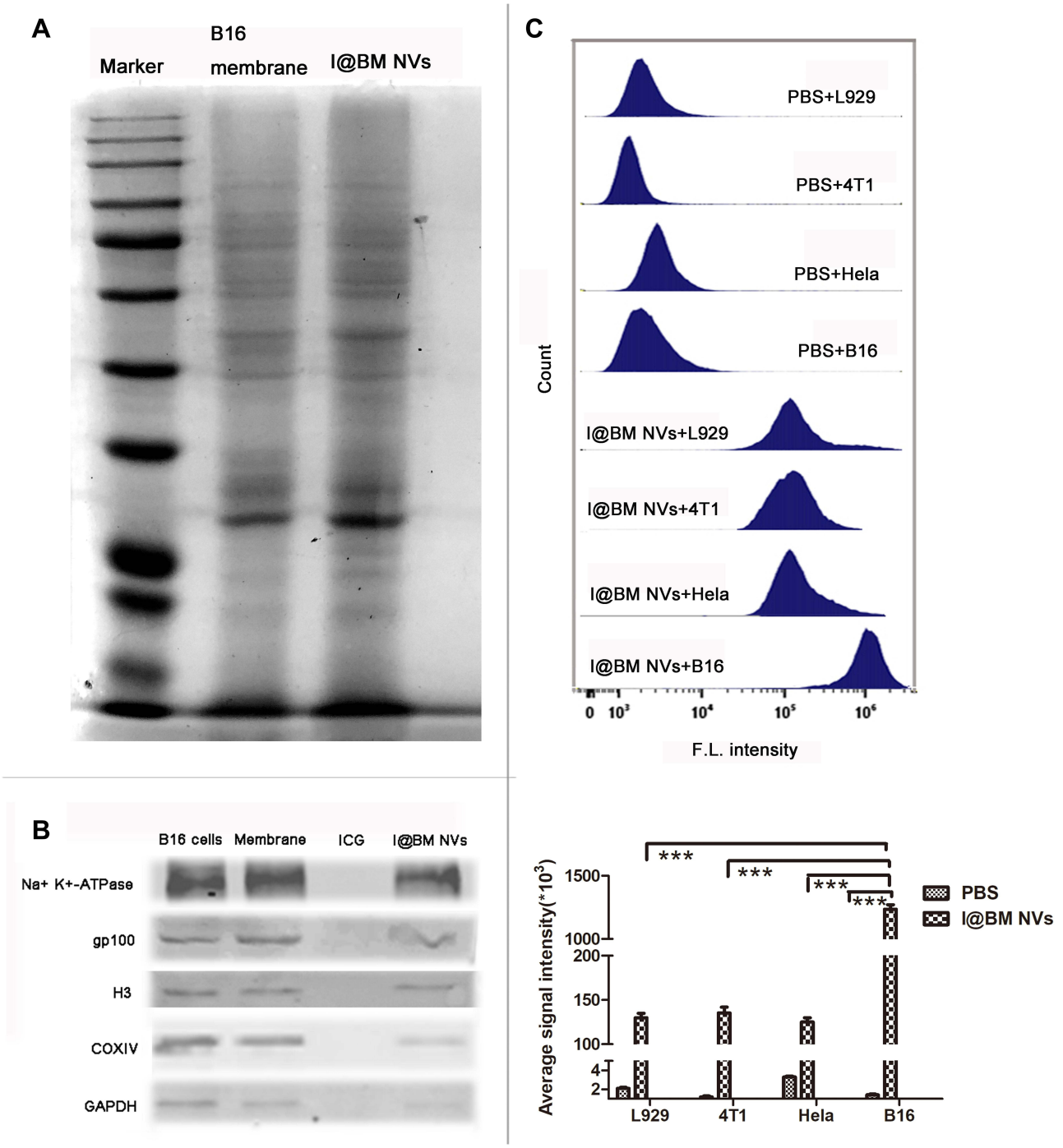

Figure 2 Validation and internalization of I@BM NVs. (**A**) SDS-PAGE analysis of cell membrane extraction and I@BM NVs. Both samples were concentrated to ensure distinct protein bands. (**B**) Western blot assay for the identification of membrane-specific and intracellular protein markers in whole cell lysate, extracted membranes, and I@BM NVs. H3, Histone H3; COXIV, cytochrome c oxidase subunit IV; GAPDH, glyceraldehyde-3-phosphate dehydrogenase. (**C**) Flow cytometry analysis showing internalization of DiD-labeled B16 cell membrane in different cells after 2 h incubation. Quantification of the mean fluorescence intensities of the histograms. Bars represent means ± SD (n = 3). P values ≤0.05 were considered to be statistically significant (***$P < 0.001$).

Cell Apoptosis

After NIR treatment, the apoptosis of B16 cells was detected by flow cytometry and western blotting. The results are shown in Figure 3C. The apoptosis rates of B16 cells in the cancer cell membrane group and the PBS group were very low, indicating that NIR light irradiation did not effectively kill cells. After 4 min of light excitation, approximately 14.7% of the B16 cells treated with ICG had undergone apoptosis, compared with about 46.2% of the B16 cells treated

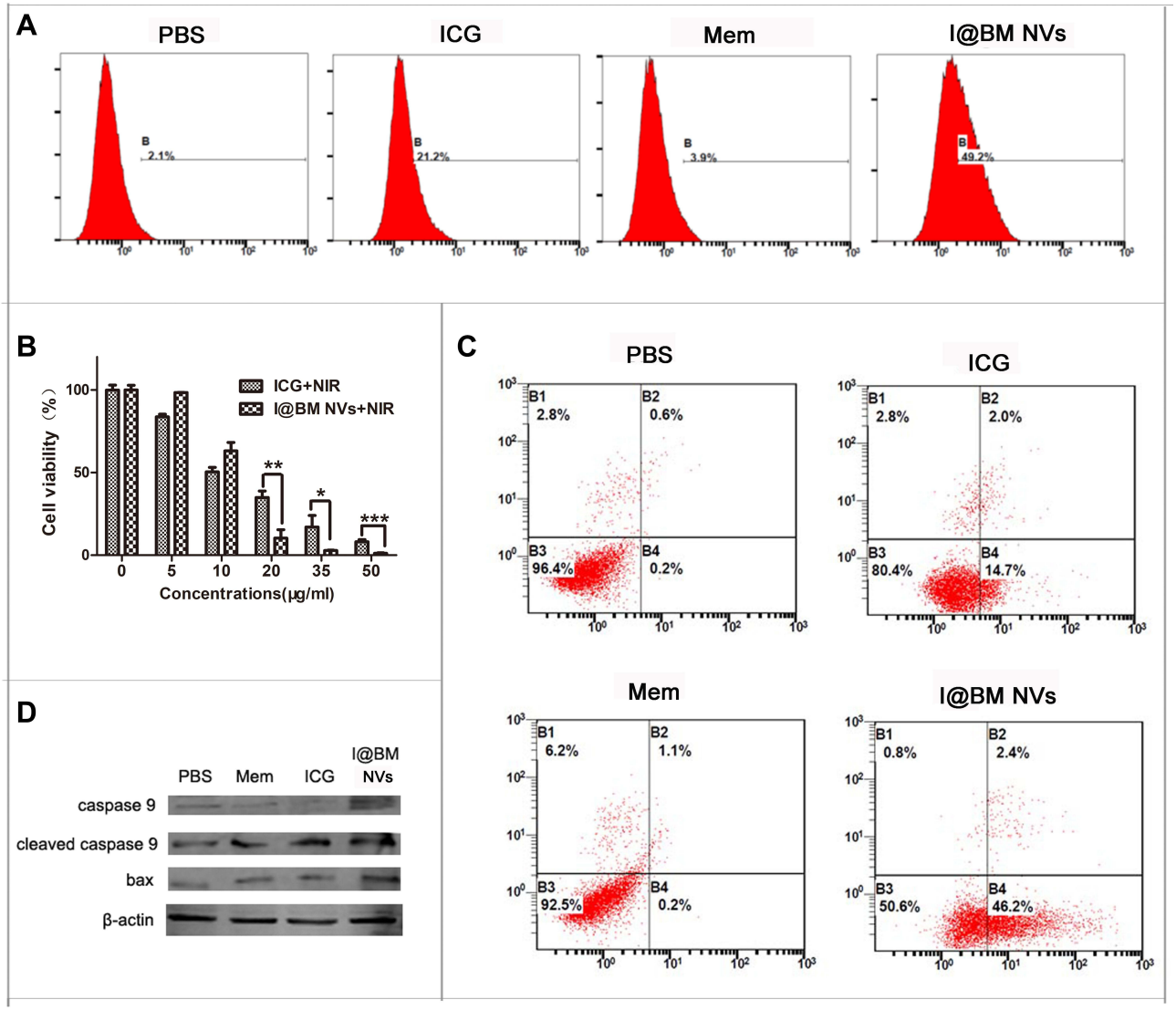

Figure 3 Cell apoptosis analysis in vitro. (**A**) Flow cytometry analysis of intracellular ROS generation. (**B**) Cell viability of B16 cells incubated with various concentrations of free ICG and I@BM NVs under NIR. (**C**) Irradiated B16 cells stained with annexin V and PI for FACS analysis. (**D**) Caspase-9 and BAX protein levels estimated by western blot analysis. Data are expressed as mean ± SD. *, ** and ***Indicate significant levels at $P < 0.05$, $P<0.01$ and $P < 0.001$, respectively.

with NVs, representing a significant difference. The homologous targeting of NVs to B16 cells and the late apoptosis of B16 cells were the main reasons for this difference. Our results were in great agreement with Hu's reports, which showed that AuNR/ICG vesicles under light excitation could produce more apoptosis of a prostate cancer cell PC3, especially inducing cells into the state of advanced apoptosis.[26] Moreover, western blotting showed that the expression levels of full-length and cleaved caspase-9 were significantly reduced and elevated, respectively. The BAX expression level also increased, which verified the induction of apoptosis (Figure 3D).

Biodistribution in B16 Tumor Model

Although both ICG and I@BM NVs could accumulate in tumors, I@BM NVs showed a higher tumor-targeting efficiency, demonstrating a clear ICG signal at 24 h post-injection (Figure 4A). Owing to their rapid cell internalization and good stability, the I@BM NVs exhibited a prominent tumor retention effect at 24 h post-injection. In addition, large amounts of free ICG accumulated in the liver and kidney (Figure 4B), whereas I@BM NVs accumulated in the liver and tumor owing to recognition of the reticulo-endothelial system.[27] Compared with free ICG, the cumulative amount of I@BM NVs in the liver and kidney was reduced by 50% and 300%, respectively, and the cumulative amount in the tumor

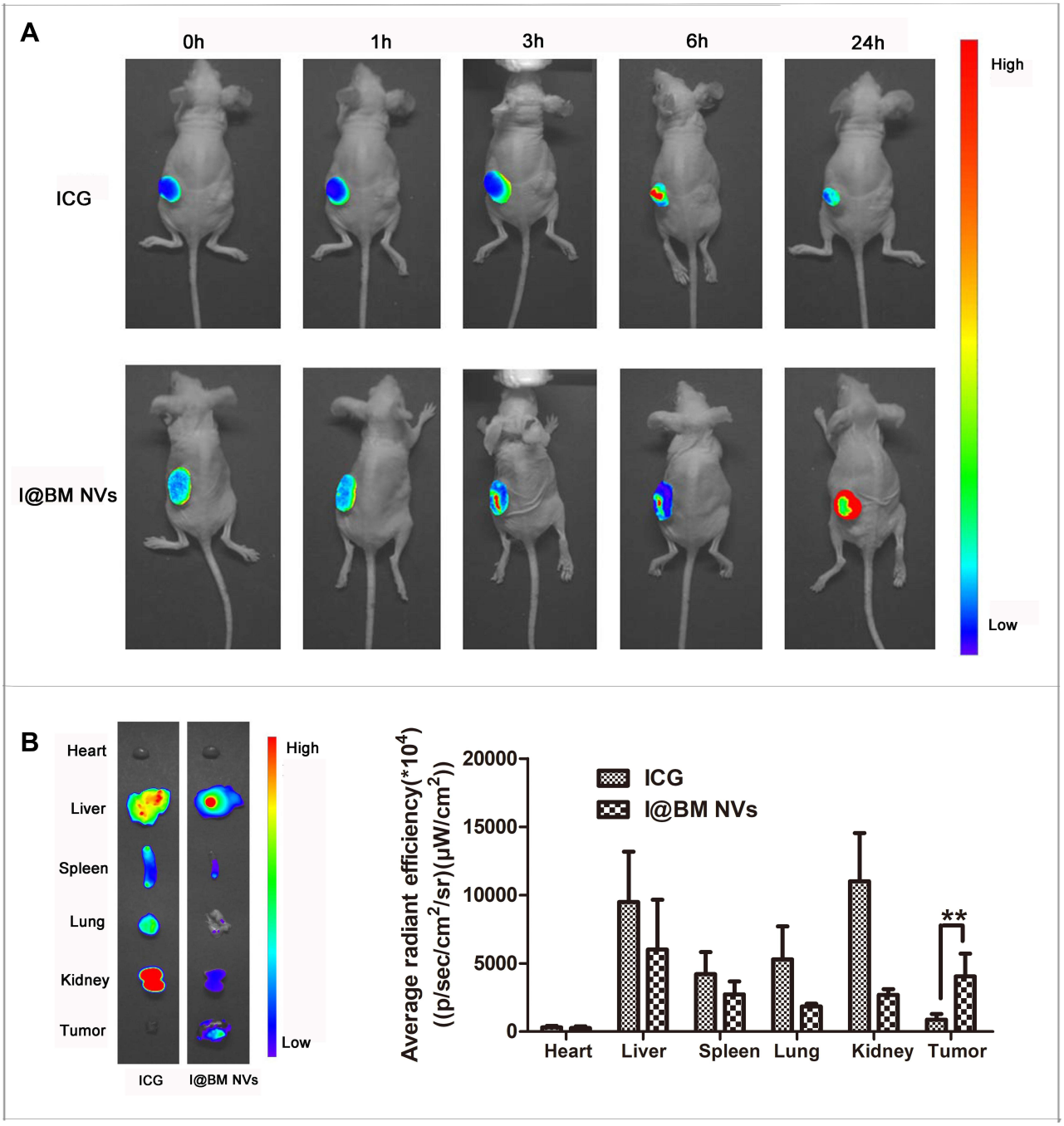

Figure 4 In vivo imaging of I@BM NVs. (**A**) Representative images of ICG and I@BM NVs at 0 min, 1 h, 3 h, 6 h, and 24 h. (**B**) Tumors and major organs after injection of free ICG and I@BM NVs at 24 h postinjection. I@BM NVs realized ideal tumor accumulation with reduced interception by the kidney and liver. And the semi-quantitative biodistribution of free ICG, I@BM NVs in nude mice was concluded by the averaged fluorescence intensity of each organ. The data are shown as mean ± SD (n = 3); **Indicates $P < 0.01$.

increased by 400%, showing a significantly enhanced tumor accumulation. This observation indicated that more B16 membrane-camouflaged ICG NVs accumulated at the tumor site after injection into the tail vein, which further verified by the tumor-targeting action of B16 membrane-camouflaged ICG NVs.

Anti-Tumor Effect of NVs

The therapeutic effect of I@BM NVs on tumor-bearing mice was further evaluated (Figure 5). Mice injected with ICG and B16 membrane had slower tumor growth rates than saline group ($P > 0.05$). However, I@BM NVs retarded the

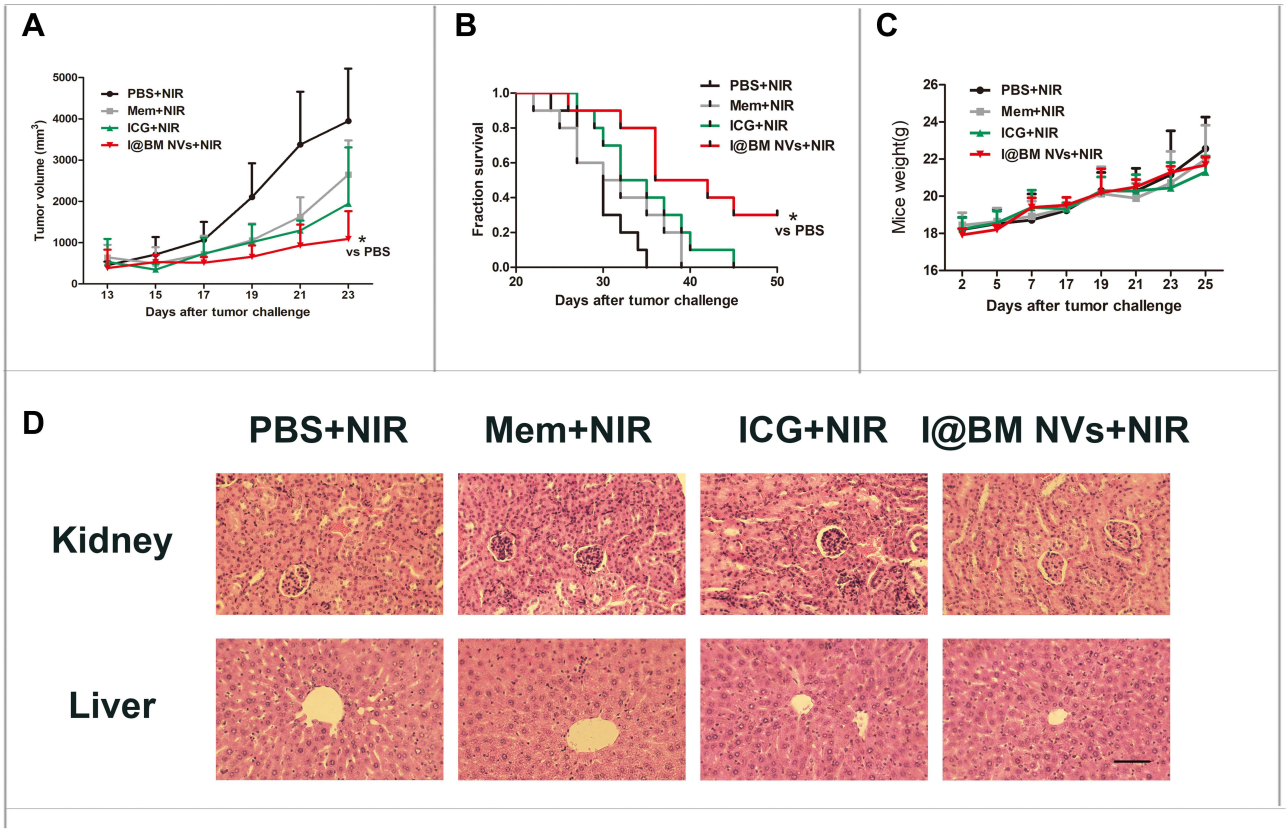

Figure 5 Therapeutic efficacy of I@BM NVs in vivo. (**A**) tumor volumes of melanoma-bearing mice after different treatments. Data are expressed as mean ± SD. * indicates $P < 0.05$. (**B**) Survival curve; each group involved 10 mice. * indicates $P < 0.05$. (**C**) Body weights of mice. Data are expressed as mean ± SD. (**D**) H&E staining of liver and kidneys tumors obtained from tumor-bearing mice (scale bar = 20 mm).

growth rates of tumors more effectively (Figure 5A). The mice injected with I@BM NVs not only had the smallest tumor sizes but also the longest survival times (Figure 5B). It is worth noting that three out of 10 mice in the I@BM NVs group survived to the end of the experiment. The weights of mice did not fluctuate significantly during the experiment (Figure 5C). There was no significant difference in histopathology between the I@BM NVs group and the other groups (Figure 5D).

One advantage of cancer cell membrane is that they carry a full array of cancer cell antigens that can stimulate an anticancer immune response.[28] The tumor microenvironment is an important factor in tumor immunity. It forms a complete ecosystem together with the tumor itself, which promotes tumor growth and metastasis while affecting immunity.[29] Overcoming the immunosuppressive effects of the tumor microenvironment can improve clinical outcomes. We analyzed immune cells in the tumor microenvironment to verify that I@BM NV stimulated the immune system to fight tumors. There was an increased number of active proliferative T cells infiltrating in the NV group. The increase in the percentage of $Ki67^+$ in $CD8^+$ and $CD4^+$ T cells in the NV group (Figure 6A) indicated an increase in numbers of active proliferative T cells in the tumor microenvironment. In addition, the numbers of MDSCs and TAMs in tumors in the I@BM NVs group were significantly reduced (Figure 6A). numbers of Tregs showed a downward trend in the experimental group compared with the control group, but the difference was not significant ($P > 0.05$) (Figure 6A). The above experimental results show that I@BM NVs activate the mouse immune system and promote the role of immune cells in killing tumors.

The decreased expression of pro-inflammatory cytokines (IL-10 and TGF-β) and the increased expression of anti-inflammatory cytokines (IL-2 and IFN-γ) reflect the transition from an immune-inhibitive state to an immune-promoting state of the tumor microenvironment (Figure 6B). Owing to the lack of a vaccine adjuvant, the NVs did not induce

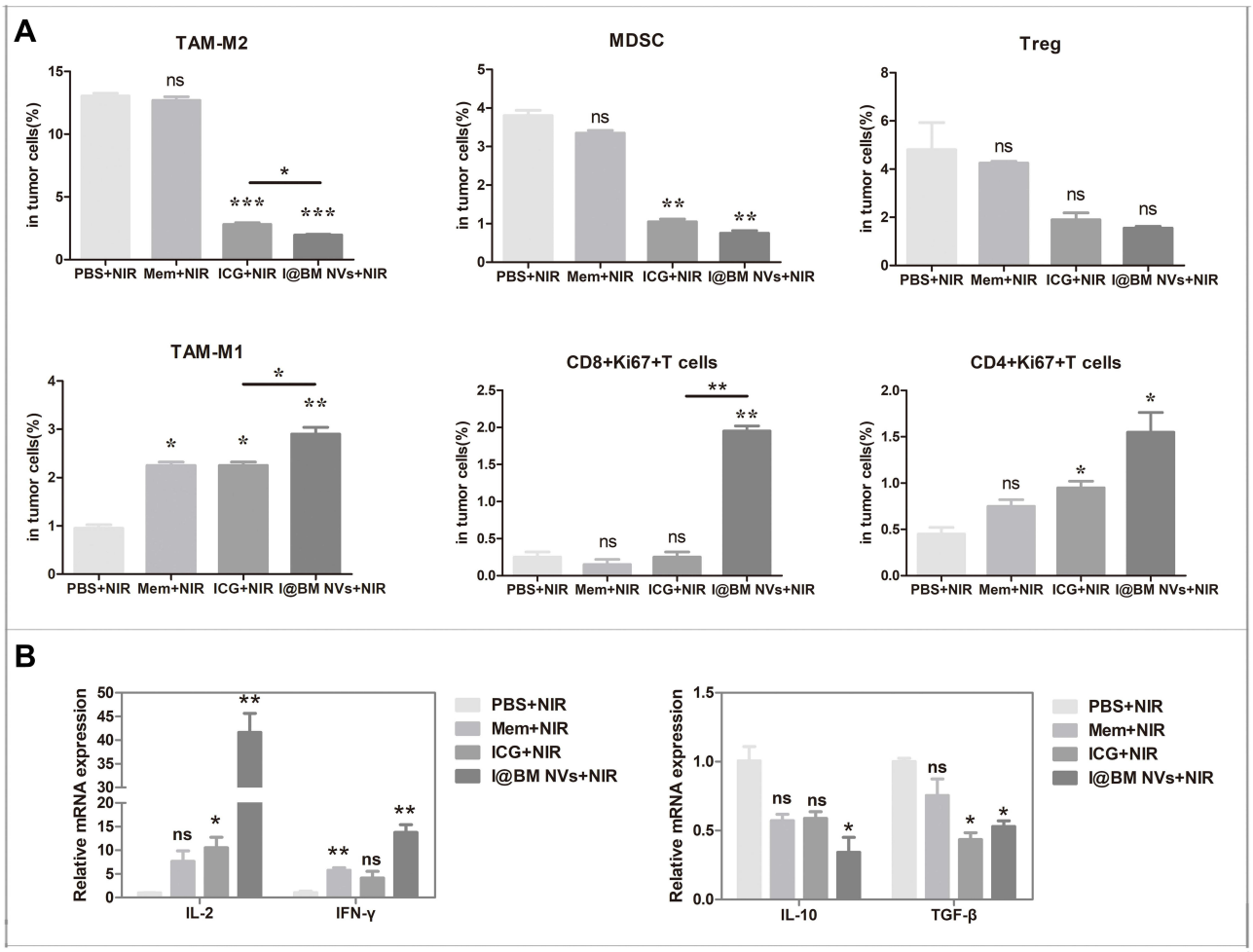

Figure 6 Evaluation of tumor microenvironment immunological markers. (**A**) Percentages of intra-tumoral immune-inhibitive (tumor-associated macrophage 2 (TAM-M2), Treg, MDSC) and immune-promoting (TAM-M1, $CD4^+Ki67^+T$, $CD8^+Ki67^+T$) cells analyzed using flow cytometry. (**B**) Relative mRNA expression of pro-tumoral and anti-tumoral cytokines analyzed using qRT-PCR. Data are expressed as mean ± SD. *, ** and ***Indicate significant levels at $P < 0.05$, $P<0.01$ and $P < 0.001$, respectively. Ns indicate not significant levels at $P>0.05$.

a strong immune response. In future work, we will add vaccine adjuvants such as MPL or R848 to enhance the anti-tumor immune response.

In general, the I@BM NVs, integrated with PDT and immunotherapy to treat melanoma, caused tumor cell apoptosis under 808-nm laser irradiation. In addition, apoptotic tumor cells, which acted as released tumor-associated antigens combined with B16 cell membrane together act as tumor antigens to elicit anti-tumor immune response. The immunotherapy effectively transformed the immunosuppressive tumor microenvironment into an immune-enhanced tumor microenvironment.

Conclusion

This approach has significant advantages, including but not limited to the low cost and simple method of synthesis, the uniform morphology and stable properties of the NVs, and their ability to effectively inhibit the tumor growth of melanoma in vivo. Our study provides new ideas and a theoretical basis for development of drugs for melanoma and other malignant tumors, as well as a new treatment method for melanoma.

Acknowledgments

This work was supported by the Jilin Scientific and Technological Development Program (Grant Nos. 20190103078JH, 20190901007JC, 20190304030YY, 20190902007TC and 20190908002TC), the Capital Construction Funds Planned Projects in the Provincial Budget of 2019 (Grant No. 2019C016), the Changchun Science and Technology Development Plan Project (Grant No. 18YJ011), and the Health Special Project of Jilin Provincial Finance Department (Grant Nos. 2019SCZ509 and 2018SCZ034). The work was also supported by a horizontal program (Grant No. 2018425).

Disclosure

The authors declare no conflict of interest.

References

1. Bray F, Ferlay J, Soerjomataram I, Siegel RL, Torre LA, Jemal A. Global cancer statistics 2018: GLOBOCAN estimates of incidence and mortality worldwide for 36 cancers in 185 countries. *CA Cancer J Clin*. 2018;68(6):394–424. doi:10.3322/caac.21492
2. Mısır AF, Durmuşlar MC, Zerener T, Gün BD. Primary malignant melanoma. *Saudi Med J*. 2016;37(4):446–449. doi:10.15537/smj.2016.4.15017
3. Naidoo C, Kruger CA, Abrahamse H. Photodynamic therapy for metastatic melanoma treatment: a review. *Technol Cancer Res Treat*. 2018;17:1533033818791795. doi:10.1177/1533033818791795
4. Dash BS, Das S, Chen JP. Photosensitizer-functionalized nanocomposites for light-activated cancer theranostics. *Int J Mol Sci*. 2021;22(13):6658. doi:10.3390/ijms22136658
5. Sakka SG, van Hout N. Relation between indocyanine green (ICG) plasma disappearance rate and ICG blood clearance in critically ill patients. *Intensive Care Med*. 2006;32(5):766–769. doi:10.1007/s00134-006-0109-6
6. Zhang D, Zhang W, Wu X, et al. Dual modal imaging-guided drug delivery system for combined chemo-photothermal melanoma therapy. *Int J Nanomed*. 2021;16:3457–3472. doi:10.2147/IJN.S306269
7. Campu A, Focsan M, Lerouge F, et al. ICG-loaded gold nano-bipyramids with NIR activatable dual PTT-PDT therapeutic potential in melanoma cells. *Colloids Surf B Biointerfaces*. 2020;194:111213. doi:10.1016/j.colsurfb.2020.111213
8. Sun Z, Wang X, Liu J, et al. ICG/l-arginine encapsulated PLGA nanoparticle-thermosensitive hydrogel hybrid delivery system for cascade cancer photodynamic-NO therapy with promoted collagen depletion in tumor tissues. *Mol Pharm*. 2021;18(3):928–939. doi:10.1021/acs.molpharmaceut.0c00937
9. Persico MG, Marenco M, De Matteis G, et al. (99m)Tc-(68)Ga-ICG-Labelledmacroaggregates and nanocolloids of human serum albumin: synthesis procedures of a trimodal imaging agent using commercial kits. *Contrast Media Mol Imaging*. 2020;2020:3629705. doi:10.1155/2020/3629705
10. Li R, He Y, Zhang S, Qin J, Wang J. Cell membrane-based nanoparticles: a new biomimetic platform for tumor diagnosis and treatment. *Acta pharmaceutica Sinica B*. 2018;8(1):14–22. doi:10.1016/j.apsb.2017.11.009
11. Le QV, Lee J, Lee H, Shim G, Oh YK. Cell membrane-derived vesicles for delivery of therapeutic agents. *Acta pharmaceutica Sinica B*. 2021;11(8):2096–2113. doi:10.1016/j.apsb.2021.01.020
12. Sushnitha M, Evangelopoulos M, Tasciotti E, Taraballi F. Cell membrane-based biomimetic nanoparticles and the immune system: immunomodulatory interactions to therapeutic applications. *Front Bioeng Biotechnol*. 2020;8:627. doi:10.3389/fbioe.2020.00627
13. Wang Y, Zhang P, Wei Y, et al. Cell-membrane-display nanotechnology. *Adv Healthcare Mater*. 2021;10(1):e2001014. doi:10.1002/adhm.202001014
14. Jin J, Krishnamachary B, Barnett JD, et al. Human cancer cell membrane-coated biomimetic nanoparticles reduce fibroblast-mediated invasion and metastasis and induce T-Cells. *ACS Appl Mater Interfaces*. 2019;11(8):7850–7861. doi:10.1021/acsami.8b22309
15. Tapeinos C, Tomatis F, Battaglini M, et al. Cell membrane-coated magnetic nanocubes with a homotypic targeting ability increase intracellular temperature due to ROS scavenging and act as a versatile theranostic system for glioblastoma multiforme. *Adv Healthcare Mater*. 2019;8(18):e1900612. doi:10.1002/adhm.201900612
16. Guo Q, Wang L, Xu P, et al. Heterologous prime-boost immunization co-targeting dual antigens inhibit tumor growth and relapse. *Oncoimmunology*. 2020;9(1):1841392. doi:10.1080/2162402X.2020.1841392
17. Gao J, Chu D, Wang Z. Cell membrane-formed nanovesicles for disease-targeted delivery. *J Control Release*. 2016;224:208–216. doi:10.1016/j.jconrel.2016.01.024
18. Gao C, Lin Z, Jurado-Sanchez B, Lin X, Wu Z, He Q. Stem cell membrane-coated nanogels for highly efficient in vivo tumor targeted drug delivery. *Small*. 2016;12(30):4056–4062. doi:10.1002/smll.201600624
19. Wei R, Jiang G, Lv M, et al. TMTP1-modified indocyanine green-loaded polymeric micelles for targeted imaging of cervical cancer and metastasis sentinel lymph node in vivo. *Theranostics*. 2019;9(24):7325–7344. doi:10.7150/thno.35346
20. Li S, Jiang W, Yuan Y, et al. Delicately designed cancer cell membrane-camouflaged nanoparticles for targeted (19)F MR/PA/FL imaging-guided photothermal therapy. *ACS Appl Mater Interfaces*. 2020;12(51):57290–57301. doi:10.1021/acsami.0c13865
21. Schwartzentruber DJ, Lawson DH, Richards JM, et al. gp100 peptide vaccine and interleukin-2 in patients with advanced melanoma. *N Engl J Med*. 2011;364(22):2119–2127. doi:10.1056/NEJMoa1012863
22. Fang RH, Hu CM, Luk BT, et al. Cancer cell membrane-coated nanoparticles for anticancer vaccination and drug delivery. *Nano Lett*. 2014;14(4):2181–2188. doi:10.1021/nl500618u
23. Peng LH, Zhang YH, Han LJ, et al. Cell membrane capsules for encapsulation of chemotherapeutic and cancer cell targeting in vivo. *ACS Appl Mater Interfaces*. 2015;7(33):18628–18637. doi:10.1021/acsami.5b05065

24. Li D, Wang Y, Li C, et al. Cancer-speci fi c calcium nanoregulator suppressing the generation and circulation of circulating tumor cell clusters for enhanced anti-metastasis combinational chemotherapy. *Acta pharmaceutica Sinica B*. 2021;11(10):3262–3271. doi:10.1016/j.apsb.2021.04.009
25. Gao Y, Zhu Y, Xu X, et al. Surface PEGylated cancer cell membrane-coated nanoparticles for codelivery of curcumin and doxorubicin for the treatment of multidrug resistant esophageal carcinoma. *Front Cell Dev Biol*. 2021;9:688070. doi:10.3389/fcell.2021.688070
26. Hu J, Luo H, Qu Q, et al. Cell membrane-inspired polymeric vesicles for combined photothermal and photodynamic prostate cancer therapy. *ACS Appl Mater Interfaces*. 2020;12(38):42511–42520. doi:10.1021/acsami.0c11636
27. Souchek JJ, Wojtynek NE, Payne WM, et al. Hyaluronic acid formulation of near infrared fluorophores optimizes surgical imaging in a prostate tumor xenograft. *Acta biomaterialia*. 2018;75:323–333. doi:10.1016/j.actbio.2018.06.016
28. Zou S, Wang B, Wang C, Wang Q, Zhang L. Cell membrane-coated nanoparticles: research advances. *Nanomedicine*. 2020;15(6):625–641. doi:10.2217/nnm-2019-0388
29. Martin JD, Cabral H, Stylianopoulos T, Jain RK. Improving cancer immunotherapy using nanomedicines: progress, opportunities and challenges. *Nat Rev Clin Oncol*. 2020;17(4):251–266. doi:10.1038/s41571-019-0308-z